JOURNAL OF MATERIALS SCIENCE 31 (1996) 4451–4466

The failure of fibre composites and adhesively bonded fibre composites under high rates of test

Part II *Mode I loading – dynamic effects*

B. R. K. BLACKMAN, A. J. KINLOCH, Y. WANG, J. G. WILLIAMS
Department of Mechanical Engineering, Imperial College of Science, Technology and Medicine, Exhibition Road, London, SW7 2BX, UK

The dynamic effects which are commonly encountered during high-rate DCB tests with fibre composite and adhesively bonded fibre composite arms have been studied in detail. This paper, Part II of the series, follows Part I, which described the experimental aspects of the high-rate testing. Part III will report the results from mode II and mixed-mode I/II tests on the fibre-composite materials.

Nomenclature

a crack length
a_0 initial crack length
$\dot{a}$ crack speed
$\ddot{a}$ crack acceleration
c longitudinal wave speed
h thickness of single arm of test specimen
p crack length perturbation (i.e. the measured value of the crack length minus the value predicted by steady-state theory)
$\dot{p}$ crack velocity perturbation
$\ddot{p}$ crack acceleration perturbation
t time
t_0 time taken for crack to initiate during the mode I test
u_0 load-line vertical displacement of single arm of test specimen ($\delta/2$ in Part I)
$u(x)$ vertical displacement of specimen at distance x from the load-line
$\dot{u}(x)$ vertical displacement rate of specimen at distance x from the load-line
x distance along the test specimen from the load-line
A constant relating the steady state crack length to root time
B width of specimen
C compliance of the specimen (u_0/P)
E_{11} axial modulus of the fibre-composite beam
G mode I energy release rate
G_{Ic} mode I critical energy release rate or fracture toughness
G_1 half the value of G_{Ic} during steady-state propagation (i.e. calculated for half the beam as shown in Fig. 1)
G_2 half the value of G_{Ic} at crack initiation
P end load applied to specimen
U_{ext} external work done
U_s strain energy
U_k kinetic energy
V velocity of a single arm of test specimen (i.e. half the measured test velocity)
β dynamic term, governed by the ratio of the energy to initiate versus that to propagate a crack
χ_I mode I crack shear deflection and root rotation correction term
Δ crack length correction term, evaluated by the negative intercept on the a versus $t^{1/2}$ plot
ε dynamic term controlling the form of the computed perturbations
ν Poisson's ratio for the fibre-composite beams
ρ density of the fibre-composite beams
τ time, normalized by the initiation time, t_0 and thus equivalent to (t/t_0)
$\bar{\tau}_n$ values of τ at which crack arrest occurs. $n = 1, 2, 3 \ldots$
ξ ratio of distance along beam to crack length (x/a)

1. Introduction

Part I [1] of this three-part series described tests on several composites to measure the mode I delamination toughness at high loading rates. It was observed that at loading rates above about $1\,m\,s^{-1}$ the load signal was so influenced by dynamic effects that it did not yield sensible values. It was concluded that the fracture toughness, G_{Ic}, was best determined from the measurement of the load-point displacement and the crack length which were measured by the use of high-speed photography. This required a knowledge of the elastic modulus, E_{11}, at these higher rates which was found to be sensibly independent of rate.

It was noted in Part I [1] that the analysis used was static and took no account of kinetic energy changes. These were estimated and found not to be large, but significant dynamic effects were observed. In particular, the high-speed camera enabled quite accurate crack length versus time data to be determined and

0022–2461

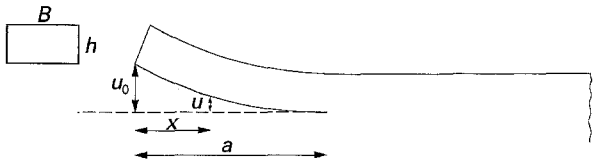

Figure 1 The model of the double-cantilever beam specimen used in the analysis. Owing to symmetry, only one arm was modelled.

hence the variation in crack speed could be monitored. These variations were found to be large and, in extreme cases, led to crack arrest and re-initiation, i.e. stick–slip propagation. Such variations have been observed in finite element results [2, 3] and attributed to dynamic effects. These effects are explained in detail in this paper with a view to establishing if they affect the accuracy of the fracture toughness values obtained. The results also give some insight into the utility of trying to characterize fracture toughness as a function of crack speed when dynamic variations occur.

2. Theory

2.1. Static analysis

Let us consider the analysis of half of the double-cantilever beam (DCB) specimen; as shown in Fig. 1 with an end deflection of u_0 and a crack length of a, the beam has a width of B. The mode I energy release rate, G for the usual double-cantilever beam test is retrieved from the results for this case by doubling the value of G and replacing u_0 with $\delta/2$, where δ is the total end deflection. The value of G, for all the cases discussed here, is derived in the usual way from [4]

$$G = \frac{1}{B}\left(\frac{dU_{ext}}{da} - \frac{dU_s}{da} - \frac{dU_k}{da}\right) \quad (1)$$

where U_{ext} is the external work, U_s is the strain energy, and U_k is the kinetic energy. The static analysis assumes that $U_k = 0$ and here we have

$$G = \frac{1}{B}\left(\frac{dU_{ext}}{da} - \frac{dU_s}{da}\right) = \frac{P^2}{2B}\frac{dC}{da} \quad (2)$$

where P is the end load and C is the compliance, u_0/P. Thus

$$C = \frac{u_0}{P} = \frac{4a^3}{Bh^3E_{11}} \quad (3)$$

where E_{11} is the axial modulus. (The various corrections for simple beam theory, which were discussed in Part I [1], will initially be omitted for clarity in what follows, but will be added in the final result.) Differentiating Equation 3 and substituting for P in Equation 2, we have

$$G = \frac{3E_{11}h^3}{8}\frac{u_0^2}{a^4} \quad (4)$$

i.e the usual result, as used in Part I, but written for half the beam as shown in Fig. 1.

For the tests used here, $u_0 = Vt$, where V is the test velocity, and is a constant for each test. Therefore, if we assume that the material has a constant toughness, G_1, then during propagation the relationship between the crack length, a, and the time, t, may be written as

$$a^4 = \left(\frac{3}{8}\frac{E_{11}h^3V^2}{G_1}\right)t^2 \quad (5)$$

i.e.

$$a = At^{1/2}$$

where A is a constant given by

$$A^4 = \left(\frac{3}{8}\frac{E_{11}h^3V^2}{G_1}\right) \quad (6)$$

It should be noted that the end rotation correction requires that

$$a + \chi_1 h = At^{1/2} \quad (7)$$

and the procedure for evaluating this correction term will be discussed in Section 3.

This is steady-state propagation [5] and assumes that at $t = 0$, $a = 0$. For practical tests there is always an initial crack length, a_0, so that in this static case the crack will initiate at

$$t_0 = \left(\frac{a_0}{A}\right)^2 \quad (8)$$

and at a velocity of

$$\dot{a}_0 = \frac{A}{2t_0^{1/2}} = \frac{a_0}{2t_0} \quad (9)$$

2.2. Dynamic effects

Exact solutions including the kinetic energy are uncommon for beam problems because of the nature of the equation of motion [6]. Useful approximations, however [7], can be obtained via the "Berry Method" where the static displacement profile is assumed, the velocities derived, and hence U_k computed. For the beam in Fig. 1

$$u = u_0\left(1 - \frac{3}{2}\frac{x}{a} + \frac{1}{2}\frac{x^3}{a^3}\right) \quad (10)$$

where x is the distance along the beam, as defined in Fig. 1.

Now, there are two cases of interest. Firstly, prior to crack initiation the crack velocity is zero, and hence

$$\dot{u} = V\left(1 - \frac{3}{2}\xi + \frac{1}{2}\xi^3\right) \quad (11)$$

where

$$\xi = \frac{x}{a} \quad (12)$$

and hence the kinetic energy may be calculated via

$$U_k = \frac{1}{2}\rho BhaV^2\int_0^1\left(1 - \frac{3}{2}\xi + \frac{1}{2}\xi^3\right)^2 d\xi \quad (13)$$

Writing the solution in the appropriate form for the energy balance we have

$$\frac{1}{B}\frac{dU_k}{da} = \frac{33}{280}E_{11}h\left(\frac{V}{c}\right)^2 \quad (14)$$

where c is the longitudinal wave speed in the composite arms and is given by

$$c = \left(\frac{E_{11}}{\rho}\right)^{1/2} \quad (15a)$$

for plane stress conditions, and

$$c\left[\frac{E_{11}}{\rho(1-\nu^2)}\right]^{1/2} \quad (15b)$$

for plane strain conditions as exist in the tests, where ρ is the density and ν is Poisson's ratio for the arms of the beam.

Secondly, for steady-state crack propagation, there is a velocity contribution from the crack motion, so

$$\dot{u} = \frac{du}{dt} + \dot{a}\frac{du}{da}$$

$$= V(1 - \tfrac{3}{2}\xi + \tfrac{1}{2}\xi^3) + V\left(\frac{\dot{a}t}{a}\right)\tfrac{3}{2}(\xi - \xi^3) \quad (16)$$

and because

$$a = At^{1/2} \quad (17a)$$

$$\frac{\dot{a}t}{a} = \frac{1}{2} \quad (17b)$$

and

$$\dot{u} = V(1 - \tfrac{3}{4}\xi - \tfrac{1}{4}\xi^3) \quad (17c)$$

proceeding as before we can compute the kinetic energy term as

$$\frac{1}{B}\frac{dU_k}{da} = \frac{111}{560}E_{11}h\left(\frac{V}{c}\right)^2 \quad (18)$$

This expression is greater than the static case (i.e. when $\dot{a} = 0$) by a factor of 1.7.

Thus, we have two expressions for G by using Equation 1. Firstly, when $\dot{a} = 0$

$$G = \left(\frac{3}{8}\frac{E_{11}h^3V^2}{a^4}\right)t^2 - \left(\frac{33}{280}\frac{E_{11}hV^2}{c^2}\right) \quad (19a)$$

and secondly when $\dot{a} > 0$

$$G = \left(\frac{3}{8}\frac{E_{11}h^3V^2}{a^4}\right)t^2 - \left(\frac{111}{560}\frac{E_{11}hV^2}{c^2}\right) \quad (19b)$$

The crack will initiate at $G = G_1$, with $\dot{a} = 0$, via Equation 19a. However, the G required for steady-state propagation, via Equation 19b will be less than the value of G_1 owing to the greater kinetic energy term in this case. Therefore, there will be a transition growth region before the crack reaches its steady-state condition. When the steady-state condition is reached we can again write

$$a = At^{1/2} \quad (7)$$

but the value of A is now given by

$$A^4 = \frac{3}{8}E_{11}h^3V^2\left[G_1 + \frac{111}{560}E_{11}h\left(\frac{V}{c}\right)^2\right]^{-1} \quad (20)$$

i.e. including the kinetic energy term for the crack growing under steady-state conditions. As Equation 20 represents the definition of A when $\dot{a} > 0$, it is now necessary to reformulate the expression for the initiation time, t_0, because the crack velocity up to this point is, of course, zero. Hence, we can write

$$t_0 = \left(\frac{a_0}{A}\right)^2\left\{\left[G_1 + \frac{33}{280}E_{11}h\left(\frac{V}{c}\right)^2\right]\Big/\left[G_1 + \frac{111}{560}E_{11}h\left(\frac{V}{c}\right)^2\right]\right\}^{1/2} \quad (21)$$

However, this analysis does not allow any details of the transition to be computed, because it assumes only two conditions, i.e. $\dot{a} = 0$ or the steady state.

2.3. Transient effects

To analyse the details of transient effects we return to the general expression for u

$$\dot{u} = V[1 - \tfrac{3}{2}(1 - n)\xi + \tfrac{1}{2}(1 - 3n)\xi^3] \quad (22)$$

where

$$n = \frac{\dot{a}t}{a} \quad (23)$$

The kinetic energy may now be computed as before

$$U_k = \tfrac{3}{280}(11 + 11n + 8n^2)E_{11}Bha\left(\frac{V}{c}\right)^2 \quad (24)$$

Noting that

$$a\frac{dn}{da} = (1 - n) + \frac{\ddot{a}t}{a} \quad (25)$$

we can write an expression for the kinetic energy when the crack is in the transition region between $\dot{a} = 0$ and the steady state as

$$\frac{1}{B}\frac{dU_k}{da} = \frac{3E_{11}h\left(\frac{V}{c}\right)^2}{280}\left[22 + 16\left(\frac{\dot{a}t}{a}\right) - 8\left(\frac{\dot{a}t}{a}\right)^2 + 11\left(\frac{\ddot{a}t}{\dot{a}}\right) + 16\left(\frac{\ddot{a}t}{a}\right)^2\right] \quad (26)$$

and because

$$G = \frac{3}{8}\frac{E_{11}h^3V^2t^2}{a^4} - \frac{1}{B}\frac{dU_k}{da} \quad (27)$$

we have an equation of motion for a when $G = G_1$. Approximate solutions to this somewhat intractable result may be deduced by considering small perturbations, p, from the steady state

$$a = At^{1/2} + p \quad (28)$$

which gives the equation of motion

$$\frac{8}{3}\left(\frac{G_1}{E_{11}h}\right)\left(\frac{c}{V}\right)^2 + \frac{37}{70} - \frac{(ch)^2}{A^4} = \frac{-38}{35At^{1/2}}\left[\frac{70}{19}\frac{(hc)^2}{A^4}p + \tfrac{1}{2}\dot{p}t + \ddot{p}t^2\right] \quad (29)$$

The left-hand side of this equation is zero for the steady state from Equation 26, and hence for small perturbations, Equation 29 reduces to

$$\ddot{p}t^2 + \tfrac{1}{2}\dot{p}t + \alpha p = 0 \quad (30)$$

where

$$\alpha = \frac{70}{19}\frac{(hc)^2}{A^4} = \frac{70}{19}\left[\frac{37}{70} + \frac{8}{3}\left(\frac{G_1}{E_{11}h}\right)\left(\frac{c}{V}\right)^2\right] \quad (31)$$

This equation has the solution of the form

$$p \propto t^{1/4 \pm i\varepsilon}$$

with

$$\varepsilon = 1.37\left[1 + 5.21\left(\frac{G_1}{E_{11}h}\right)\left(\frac{c}{V}\right)^2\right]^{1/2} \quad (32)$$

which has a real part of

$$p = \left(\frac{t}{t_0}\right)^{1/4}\left[Y_1 \sin\left(\varepsilon \ln\frac{t}{t_0}\right) + Y_2 \cos\left(\varepsilon \ln\frac{t}{t_0}\right)\right] \quad (33)$$

and

$$\dot{p} = \frac{1}{t_0}\left(\frac{t}{t_0}\right)^{-3/4}\left[\left(\frac{Y_1}{4} - \varepsilon Y_2\right)\sin\left(\varepsilon \ln\frac{t}{t_0}\right) + \left(\frac{Y_2}{4} + \varepsilon Y_1\right)\cos\left(\varepsilon \ln\frac{t}{t_0}\right)\right] \quad (34)$$

where Y_1 and Y_2 are constants. The boundary conditions are set at $t = t_0$, because the form is indeterminate at $t = 0$. Now t_0 is determined from Equation 21 and here

$$p_0 = (a_0 - At_0^{1/2}) = a_0(1 - \beta) \quad (35a)$$

and

$$\dot{p}_0 = -\frac{\beta a_0}{2t_0} \quad (35b)$$

because $\dot{a} = 0$ at initiation
where

$$\beta = \left\{\left[G_1 + \frac{33}{280}E_{11}h\left(\frac{V}{c}\right)^2\right]\Big/\left[G_1 + \frac{111}{560}E_{11}h\left(\frac{V}{c}\right)^2\right]\right\}^{1/4} \quad (36)$$

Substituting these results gives:

$$Y_1 = -\frac{a_0}{4\varepsilon}(1 + \beta) \quad (37a)$$

$$Y_2 = a_0(1 - \beta) \quad (37b)$$

and therefore

$$\frac{p}{a_0} = \tau^{1/4}\left[(1 - \beta)\cos(\varepsilon \ln\tau) - \left(\frac{1 + \beta}{4\varepsilon}\right)\sin(\varepsilon \ln\tau)\right] \quad (38)$$

and

$$\frac{t_0\dot{p}}{a_0} = \frac{-\tau^{-3/4}}{2}\left\{\beta\cos(\varepsilon \ln\tau) + \left[\left(\frac{1 + \beta}{8\varepsilon}\right) + 2\varepsilon(1 - \beta)\right]\sin(\varepsilon \ln\tau)\right\} \quad (39)$$

where $\tau = t/t_0$.

The mismatch of boundary conditions with the steady state at initiation leads to non-linear oscillations in p and $\dot{p}$ and it will be shown in Sections 3 and 4 that Equations 38 and 39 quite accurately predict the measured crack behaviour in the high-rate DCB tests.

2.4. "Stick–slip" crack growth

The physical origins of "stick–slip" crack growth can be from various sources, but in the DCB test it can be modelled by assuming that at initiation $\dot{a} = 0$, $G = G_2 > G_1$, and $\dot{a} > 0$, $G = G_1$, as before.

The definition of A remains as in Equation 20, because the steady state is unaltered but we simply change the definition of β

$$\beta = \left\{\left[G_2 + \frac{33}{280}E_{11}h\left(\frac{V}{c}\right)^2\right]\Big/\left[G_1 + \frac{111}{560}E_{11}h\left(\frac{V}{c}\right)^2\right]\right\}^{1/4} \quad (40)$$

and

$$t_0 = \left(\frac{a_0}{A}\right)^2\beta^2 \quad (41)$$

For $G_2 = G_1$ then we have $\beta < 1$, but for $G_2 > G_1$ the value of β may be greater than unity. Note that for very high test rates $\beta \to 0.88$ and $\varepsilon \to 1.37$ in all cases and for low speeds

$$\beta \to \left(\frac{G_2}{G_1}\right)^{1/4} \quad (42)$$

and $\varepsilon \to \infty$. A condition of interest in stick–slip is whether the crack will subsequently arrest after initiation. This is given by

$$\dot{a} = \frac{A}{2t_0^{1/2}}\bar{\tau}^{-1/2} + \dot{p} = 0$$

which is determined by the equation

$$\frac{e^{\omega/4\varepsilon} - \cos\omega}{\sin\omega} = \frac{1}{\beta}\left[\left(\frac{1 + \beta}{8\varepsilon}\right) + 2\varepsilon(1 - \beta)\right] \quad (43)$$

where $\omega = \varepsilon \ln\bar{\tau}$. Arrest conditions are in the range $\pi < \omega < 2\pi$ when the left-hand side is negative, which is only true for

$$\beta > \frac{16\varepsilon^2 + 1}{16\varepsilon^2 - 1} \sim 1 + \frac{1}{8\varepsilon^2} \quad (44)$$

Because ε is usually large, this condition becomes

$$\frac{G_2}{G_1} > 1 + \frac{1.2}{\varepsilon^2} \tag{45}$$

3. Analysis of the experimental test data obtained when testing the epoxy/carbon-fibre composite (continuous crack growth)

3.1. Introduction

It was shown in Part I [1] how DCB specimens prepared with either one of two polymeric-based carbon-fibre composites, or as adhesively bonded carbon-fibre composite joints were tested in mode I at rates of up to about 20 m s^{-1}. Essentially, two distinct types of crack-growth behaviour were reported. The first type, which was exhibited for crack growth in the epoxy/carbon-fibre composite, was stable with the crack growing in a more or less continuous manner, subject to dynamic variation, after initiation until complete failure. The second type, shown by the PEEK/carbon-fibre composite and the adhesive joints at faster rates, was unstable with the crack growing in a stick–slip manner. In this section, it will be shown how the dynamic analysis has been applied to the experimental data recorded for the epoxy/carbon-fibre composite. Section 4 will show how the analysis may be applied to the experimental data recorded for the PEEK/carbon-fibre composite, which showed stick–slip crack growth. The adhesive joint test data are analysed in Section 5.

The measurement of the crack length, a, and the load point opening displacement, u_0 or δ, as a function of time was described in detail in Part I [1] for DCB tests conducted at rates of up to about 20 m s^{-1}. The measured experimental parameters were analysed statically using Equation 4, which was corrected for the various effects discussed previously and values of the mode I fracture toughness, G_{Ic}, were calculated. It was also noted in Part I [1] that under various circumstances, highly transient values of the measured crack length, a, and crack velocity, $\dot{a}$, were recorded. In the following, the experimental data will be analysed by the dynamic analysis presented in Sections 2.2 and 2.4 to calculate values of G_{Ic} which are corrected for kinetic energy. Then the transient analysis presented in Section 2.3 will be employed and it will be shown how the dynamic variation in the measured values of a and $\dot{a}$ may be predicted. In the following sections the test rates referred to are the actual specimen displacement rates as recorded by high-speed photography. It was noted in Part I [1] that at high test rates, this value may be different from the actual ram displacement rate.

3.2. Interpretation of the epoxy/carbon-fibre composite experimental data

The static analysis of the experimental data measured for the epoxy/carbon-fibre composite showed that the value of G_{Ic} was approximately independent of test rate up to about 20 m s^{-1}. However, tests conducted

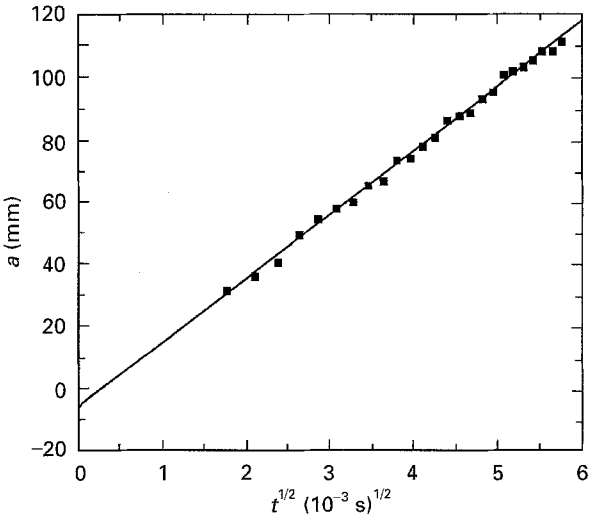

Figure 2 Crack length versus root time values for a test conducted at a rate of 0.65 m s^{-1} with the epoxy/carbon-fibre composite. The linear fit to the data yields a correlation coefficient of 0.997.

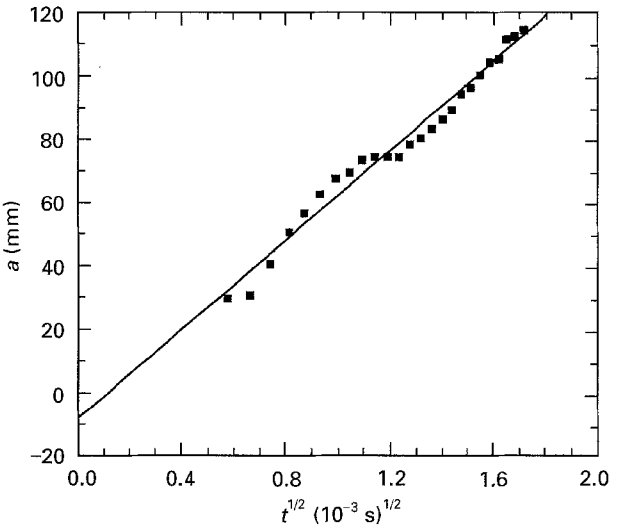

Figure 3 Crack length versus root time values for a test conducted at a rate of 8 m s^{-1} with the epoxy/carbon-fibre composite. The linear fit to the data yields a correlation coefficient of 0.978.

at the faster rates showed some curious dynamic effects which will now be discussed. It was shown in Section 2.1 that a linear relationship exists between the crack length, a, and $t^{1/2}$. Hence a graph of a versus $t^{1/2}$ is linear with gradient A, which is defined by Equation 6 in the static case and Equation 20 in the dynamic case. Equation 20 describes crack propagation, so only crack propagation data should be included in the a versus $t^{1/2}$ plots. Figs 2 and 3 show plots of a versus $t^{1/2}$ for the epoxy/carbon-fibre composite tested at 0.65 and 8 m s^{-1}, respectively. Only propagation data points are included in these figures and straight lines have been drawn though the data using a least squares regression technique. The linear fit to the data is excellent for the test conducted at 0.65 m s^{-1}, i.e. the correlation coefficient is 0.997. The test data at 8 m s^{-1} show more dynamic variation and the linear fit to these data has a correlation coefficient of 0.978. The value of the gradient, A, obtained in each case can be put into Equation 20 and a value of

TABLE I Experimental values of A, Δ and t_0 for the epoxy/carbon-fibre composite at increasing test rates with the corresponding values of G_1 and G_2

Test rate ($m\,s^{-1}$)	Expt. A ($mm\,(ms)^{-1/2}$)	Δ (mm)	Expt. t_0^a (ms)	G_1 ($J\,m^{-2}$) (Eq. 20)	G_2 ($J\,m^{-2}$) (Eq. 40)
0.65	20.6	5.9	3.76 ± 0.63	148	191
7.50	64.9	6.5	0.44 ± 0.05	186	294
8.00	71.1	8.7	0.32 ± 0.05	156	265
20.50	109.7	16.9	0.13 ± 0.05	138	252

[a] Errors represent the high-speed camera framing interval.

G_1 may then be deduced as all the other terms in this equation are known or can be calculated. It should be noted that the model considers one arm of the DCB only and therefore the velocity, V, in the analysis is half the actual recorded test velocity. Also, G_1 and G_2 represent half the values associated with the whole beam. Hence, it is always necessary to double the values of G_1 and G_2 when comparing with previously published values of G_{Ic}.

It was noted in Equation 7 that, in practice, it is the relationship between $a + \chi h$ versus $t^{1/2}$ that is linear and so a graph of a versus $t^{1/2}$ will also be linear with gradient A, but will intercept the a axis at a negative value. Therefore, the value of the negative intercept can be taken as an approximation to the value of χh for each test and here this parameter will be referred to as Δ. It can be seen that the linear fit to the propagation data for the epoxy/carbon-fibre composite shown in Fig. 2 has yielded a gradient, $A = 20.6\,mm\,(ms)^{-1/2}$ and the negative intercept yields a value of $\Delta = 5.9$ mm. The values of A, Δ and the corresponding values of G_1 are shown in Table I for the epoxy/carbon-fibre composite at four different test rates between 0.65 and 20.5 $m\,s^{-1}$.

The value of G_1 produced by this procedure is the steady state value of G_{Ic}, i.e. it is the value of G_{Ic} obtained by assuming that $a + \Delta = At^{1/2}$. However, it was shown in Part I [1] and will be shown again later, that the experimentally recorded value of a shows a dynamic variation and oscillates about the value predicted by the steady state. This oscillation can be seen in Fig. 2 but is more noticeable in Fig. 3 where the test velocity was higher. The variation in the measured crack length values will introduce a variation into the calculated values of G when either Equation 4 or 19 is used. Fig. 4 shows the values of applied G calculated for the test at 0.65 $m\,s^{-1}$. The values of G deduced via Equations 4 and 19 were coincident at this test rate. Also shown on this figure is the value of G_1, i.e. the value of G deduced by assuming steady-state crack growth, i.e. as deduced from Equation 20 with the previously determined value of A. It can be seen that the variation in a introduces a variation in G, and at crack initiation a much higher value of G is calculated using either Equation 4 or 19. Fig. 5 shows similar data for a test at 8 $m\,s^{-1}$. The variation in applied G calculated using either Equation 4 or Equation 19 is more severe at this higher rate and again the value of G at crack initiation is higher than for subsequent propagation. In Part I this was

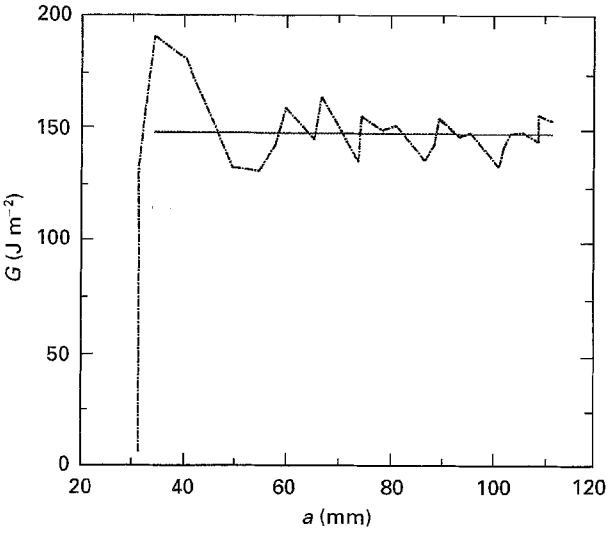

Figure 4 Values of applied G, calculated for the epoxy/carbon-fibre composite at a test rate of 0.65 $m\,s^{-1}$. (a) (· · ·) Static analysis (Equation 4), (b) (– – –) dynamic analysis (Equation 19), (c) (——) steady-state theory. Note that Equations 4 and 19 are coincident at this low test rate.

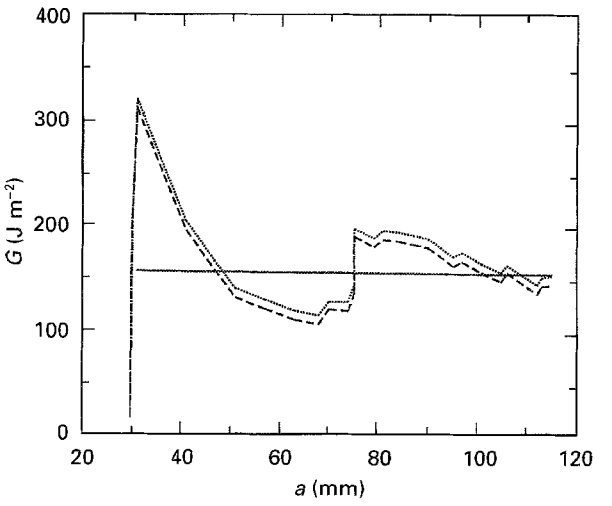

Figure 5 Values of applied G, calculated for the epoxy/carbon-fibre composite at a test rate of 8 $m\,s^{-1}$. (a) (· · ·) Static analysis (Equation 4), (b) (– – –) dynamic analysis (Equation 19), (c) (——) steady-state theory.

attributed to a dynamic effect, and the value of G_{Ic} quoted for the epoxy/carbon-fibre composite at the higher test rates was obtained by averaging the propagation values of G after the initial dynamic effect. However, the dynamic analysis derived in Section 2 distinguishes between the value of G_{Ic} at crack initiation, termed $2G_2$, and the value of G_{Ic} for crack propagation, termed $2G_1$. Therefore, in order to apply the analysis to these experimental data, it was necessary to accommodate the need for the higher value of G_{Ic} at crack initiation. We shall return later to discuss the reasons why $G_2 > G_1$. An important point here is that it is unlikely that G_2 represents a material property as its value depends on the nature of the initial crack and on another system factor that will be discussed later. However, the value of G_1 is the fracture toughness for crack propagation and is a material property.

The values of test velocity in Table I are the actual experimental test velocities used, but the values of

G_1 and G_2 are the values associated with a single-cantilever beam as shown in Fig. 1 and therefore need to be doubled when considering the double-cantilever beam. The analysis of the high-speed films enabled a measurement of the crack initiation time, t_0, to be made. This value is also shown in Table I. Experimentally, the value of t_0 was obtained by defining the two frames between which crack initiation occurred and then taking the initiation time as the time in the middle of this range. The errors indicate, therefore, the maximum and minimum possible values of t_0 and, therefore, the magnitude of the errors are dependent upon the framing rate of the camera. The camera was operated at a framing rate of about 10 000 frames s^{-1} for all test rates above 2 m s^{-1}, and so the magnitude of the errors in absolute terms is constant above this rate. Of course, the percentage error in t_0 increases as the test velocity is increased, because the value of t_0 decreases with increasing test rate.

The experimentally measured values of t_0 were used to calculate the values of G_2. As discussed previously and as shown in Figs 4 and 5, it was noted that the value of G_{Ic} recorded at crack initiation was higher than the value associated with crack propagation at the higher rates, and therefore it was possible to define a value for the dynamic parameter, β, via Equation 41 because t_0, a_0 and A are now all known. Therefore, by calculating the value of β, we can compute the appropriate value of G_2 using Equation 40. Equation 40 was used to calculate β rather than Equation 36 because $G_2 > G_1$. Hence the experimentally determined values of t_0 and A were used to compute the values of β and G_2.

3.3. Relationship between the experimental data and the steady state

Steady-state values of crack length, a, and crack velocity, $\dot{a}$, can be computed using Equations 7 and 9 provided appropriate values of the gradient A and the intercept Δ are available. By writing $\chi h = \Delta$, we can compare the corrected experimental values of a, i.e. $a + \Delta$, with the values computed as $A t^{1/2}$. Figs 6 and 7 show the crack length versus time data and crack velocity versus time data plotted for the epoxy/carbon-fibre composite at a test rate of 0.65 m s^{-1}. The points on these graphs show the experimental data points, corrected by adding Δ, and the solid lines show the steady state values of a and $\dot{a}$. Figs 8 and 9 show the same data recorded for the test at 8 m s^{-1}. It is apparent from these figures that following crack initiation, the experimental values of a and $\dot{a}$ oscillate about the values predicted by the steady state, and the frequency of oscillation decreases as the test rate is increased. It was proposed earlier in Section 2 that these variations were the result of perturbations caused by the different energy requirements of the crack at initiation and during propagation. Hence the equation of motion for crack growth was solved by considering small perturbations, p, from the steady state. Here we may define the crack length perturbation as

$$p(t) = (a + \Delta)(t) - A t^{1/2} \quad (46)$$

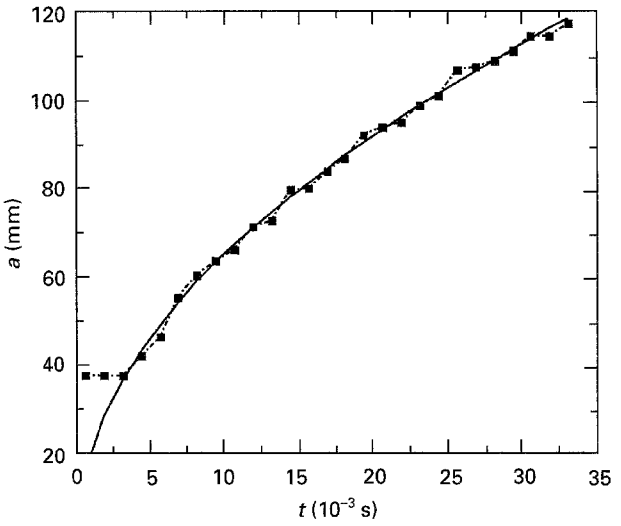

Figure 6 Crack length versus time data recorded for the epoxy/carbon-fibre composite at a test rate of 0.65 m s^{-1}. Data points represent the corrected crack length values, i.e. the experimentally measured crack length plus the correction term, Δ. (—) Values of the crack length predicted by steady-state theory.

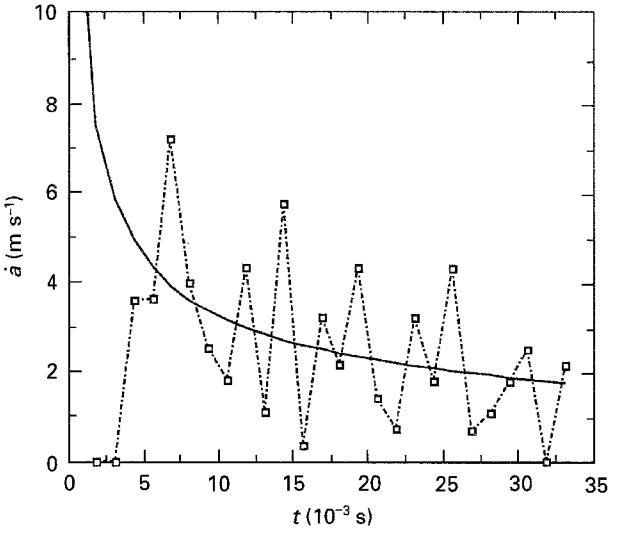

Figure 7 Crack velocity versus time data recorded for the epoxy/carbon-fibre composite at a test rate of 0.65 m s^{-1}. Data points represent the experimentally measured values. (——) Values predicted by steady-state theory.

So we can consider p to be the extent to which the measured value of the corrected crack length deviates from the steady-state value. As can be seen in Figs 6 and 8, p is not a constant, but is a non-linear function of t and will be discussed further in the next section. Considering now the crack velocity, we may define the crack velocity perturbation, $\dot{p}$, as

$$\dot{p}(t) = \dot{a}(t) - A/2t^{1/2} \quad (47)$$

Note again that $\dot{p}$ is a non-linear function of t and is independent of Δ because $\dot{a}$ is independent of Δ. We shall discuss $\dot{p}$ in more detail in the next section.

3.4. Use of the transient analysis to predict the crack-growth behaviour

It was shown in Section 2.3 that crack-growth behaviour could be predicted using Equations 38 and 39 for

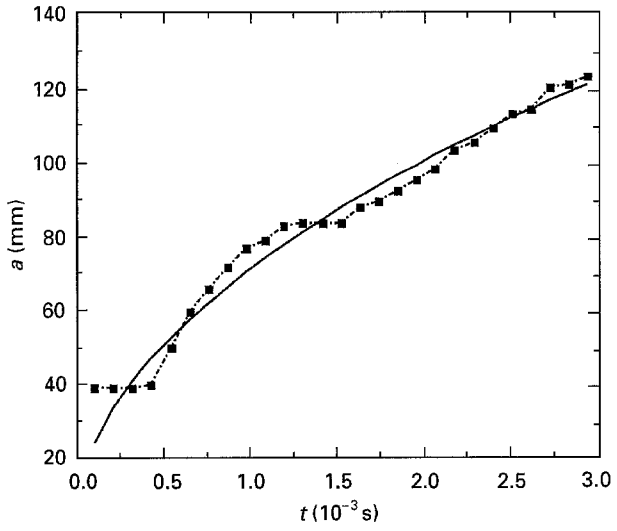

Figure 8 Crack length versus time data recorded for the epoxy/carbon-fibre composite at a test rate of 8 m s^{-1}. Data points represent the corrected crack length values. (——) Values predicted by steady-state theory.

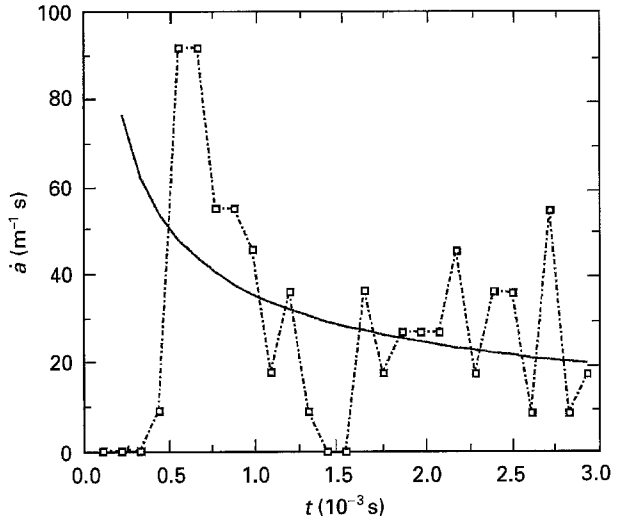

Figure 9 Crack velocity versus time data recorded for the epoxy/carbon-fibre composite at a test rate of 8 m s^{-1}. The data points represent the experimentally measured values. (——) Values predicted by steady-state theory.

a DCB test provided that the initiation time, t_0, was known and that the dynamic parameters β and ε could be calculated. Equation 38 represents a solution to the equation of motion of the crack and was formulated in terms of the crack-length perturbation, p, which was normalized by a_0. Similarly, Equation 39 gives an expression for the crack-velocity perturbation, $\dot{p}$, which was normalized by a_0/t_0, rendering the results dimensionless. In this section, the results obtained from Equations 38 and 39 will be compared to the experimental results obtained by using Equations 46 and 47. These results will also be normalized to enable comparisons to be drawn.

The values of t_0, β and ε used for the computation of Equations 38 and 39 are shown in Table II for the epoxy/carbon-fibre composite. Because there was a degree of uncertainty in the measured values of t_0 (see errors in Table I) the values of t_0 used for the computation have been allowed to vary within the confines of these errors. Table II shows the actual values of t_0 used in the computation and Table I shows the actual values of t_0 measured in the experiment.

TABLE II Calculated values of t_0, β and ε for the epoxy/carbon-fibre composite at increasing test rates

Test rate (m s^{-1})	t_0 (ms)	β (Eq. 41)	ε (Eq. 32)	ε (Best fit)
0.65	3.75	1.066	72.83	51.51
7.50	0.39	1.115	7.26	5.22
8.00	0.37	1.132	6.19	4.48
20.50	0.14	1.102	2.60	2.08

The parameter β was determined using Equation 41 and the parameter ε was determined using Equation 32. Equations 38 and 39 were computed in the range from $t = t_0$ until the time at which final failure occurred in the experiment. The computation step size was fixed to be equivalent to the experimental data recording interval. Thus, Equations 38 and 39 were calculated at time increments equivalent to the framing interval of the high-speed camera. This gave a realistic form for comparison, but the complete solutions to Equations 38 and 39 are shown in Figs 10 and 11 for the epoxy/carbon-fibre composite at a test rate of 0.65 m s^{-1}. The initial agreement between the experimentally deduced values of p/a_0 and $\dot{p}t_0/a_0$ and the computed values showed the correct form, but theory and experiment were out of phase, particularly at the higher test rates. A possible reason for this divergence will now be discussed.

The model developed in Section 2 assumed perfect symmetry of the DCB test and hence only one arm was modelled, and the results were doubled when considering the whole beam. This model is accurate at lower test rates, but at the higher test rates, e.g. above 2 m s^{-1}, analysis of the high-speed films showed that the displacement distribution between the upper and lower arms in the DCB was no longer perfectly symmetrical and the degree of asymmetry increased as the test velocity was increased. A useful insight into the effect of asymmetry in the DCB test can be obtained by considering a purely asymmetric beam displacement profile, i.e. where one arm is subjected to zero displacement and the other arm is subjected to a displacement equivalent to the total measured displacement. With this purely asymmetrical displacement, the value of G calculated would be twice the value obtained if symmetry had been assumed, i.e. the ratio of asymmetric to symmetric G is $G_{as}/G_s = 2$. In a typical test at 8 m s^{-1}, G_{as}/G_s was measured to be 1.1. In the dynamic transient analysis, this effect has been accounted for by adjusting the value of ε put into Equations 38 and 39. Rather than using the value of ε calculated by Equation 32, a value was chosen for each test which gave the best fit between the experimentally determined values of p/a_0 and $\dot{p}t_0/a_0$ and the computed values. The best fit values of ε were somewhat lower than those calculated using Equation 32

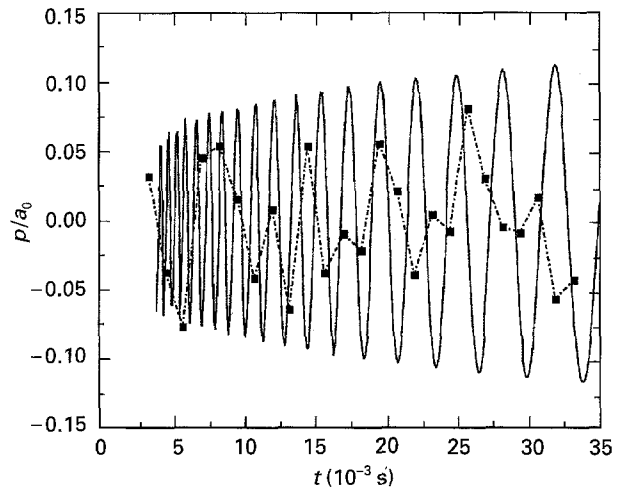

Figure 10 Values of p/a_0 versus time for the epoxy/carbon-fibre composite at a test rate of 0.65 m s^{-1}. Data points are the experimental values. (——) The analytical solution to Equation 38.

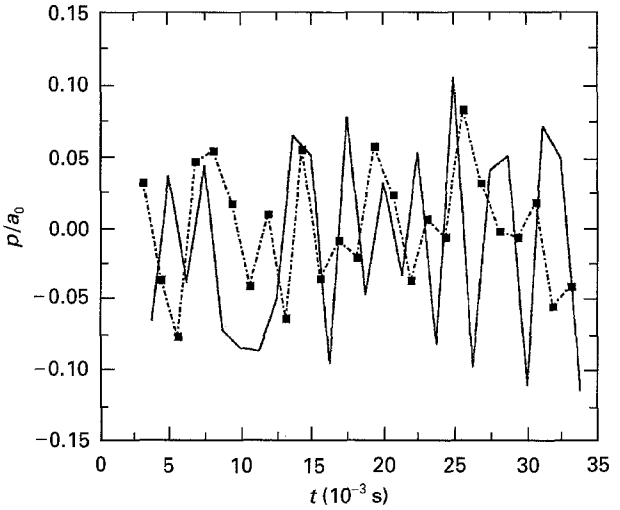

Figure 12 Values of p/a_0 versus time for the epoxy/carbon-fibre composite at a test rate of 0.65 m s^{-1}. Data points are the experimental values. (——) The solution to Equation 38, with the analytical time step now equivalent to the experimental recording interval.

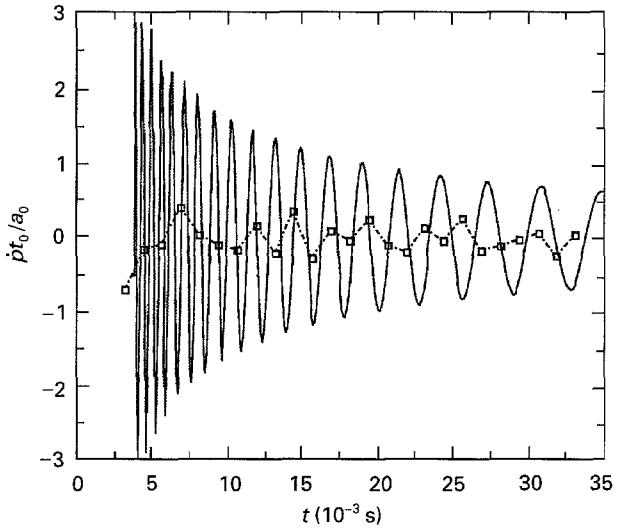

Figure 11 Values of $\dot{p}t_0/a_0$ versus time for the epoxy/carbon-fibre composite at a test rate of 0.65 m s^{-1}. Data points are the experimental values. (——) The analytical solution to Equation 39.

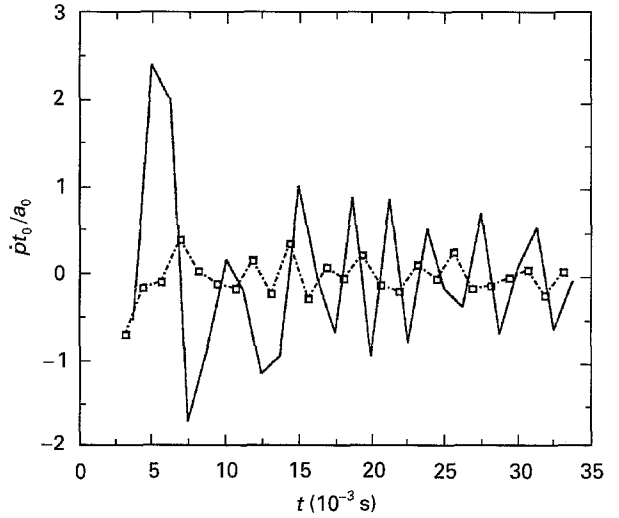

Figure 13 Values of $\dot{p}t_0/a_0$ versus time for the epoxy/carbon-fibre composite at a test rate of 0.65 m s^{-1}. Data points are the experimental values. (——) The solution to Equation 39, with the analytical time step now equivalent to the experimental recording interval.

and the values are tabulated in Table II for the epoxy composite.

Equations 38 and 39 were computed with the new values of ε and these values are plotted in Figs 12 and 13, respectively, for the epoxy/carbon-fibre composite tested at 0.65 m s^{-1}, and in Figs 14 and 15 for the test conducted at 8 m s^{-1}. It can be seen that the values of p/a_0 and $\dot{p}t_0/a_0$ obtained from experiment and theory show quite good agreement, particularly at 8 m s^{-1}. Hence, the transient crack length and crack-velocity behaviour can be quite accurately predicted using the dynamic analysis. The oscillation in a and $\dot{a}$ causes an oscillation in G of the type that has been reported elsewhere [2, 3]. The value of G for steady-state propagation, G_1, was obtained from a linear fit to the a versus $t^{1/2}$ data and hence this is an average propagation value of G_{Ic}. The measured value of G using a static analysis fluctuates about this value at high test rates. Table I shows that the dynamic value of G_{Ic} for steady-state propagation ($\equiv 2G_1$) remained essentially constant with increasing test rate up to 20 m s^{-1}. However, at these high test rates, the value of G_{Ic} at initiation ($\equiv 2G_2$) was higher than for subsequent propagation. This was confirmed by both the R-curves and the measured values of t_0, which both suggested that $G_2 > G_1$ at high rates. Further, by using these values of G in the model, the form of the measured crack-growth behaviour was quite accurately predicted. In the next section, stick–slip crack growth will be considered.

4. Analysis of the experimental test data obtained when testing the PEEK/carbon-fibre composite (stick–slip crack growth)

4.1. Introduction

In Section 3 the dynamic analysis was applied to crack growth in the epoxy/carbon-fibre composite which

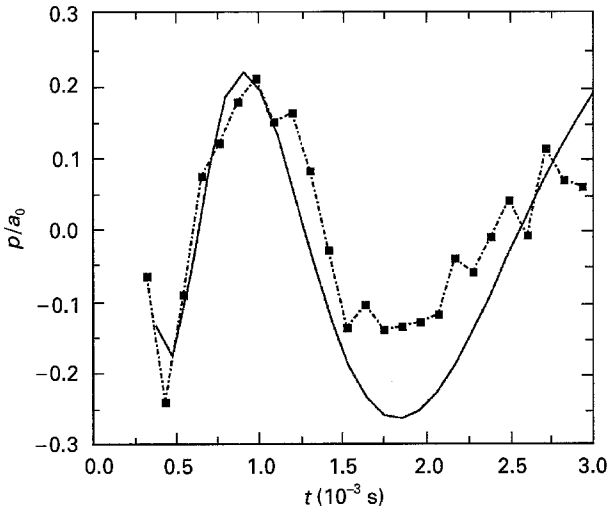

Figure 14 Values of p/a_0 versus time for the epoxy/carbon-fibre composite at a test rate of 8 m s^{-1}. Data points are the experimental values. (—) Equation 38.

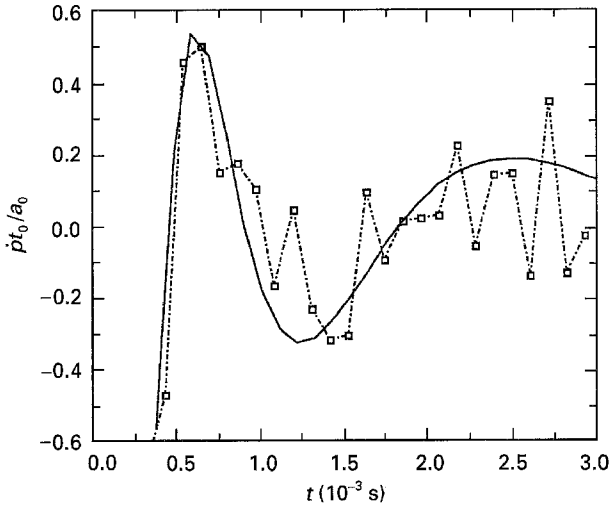

Figure 15 Values of $\dot{p}t_0/a_0$ versus time for the epoxy/carbon-fibre composite at a test rate of 8 m s^{-1}. Data points are the experimental values. (—) Equation 39.

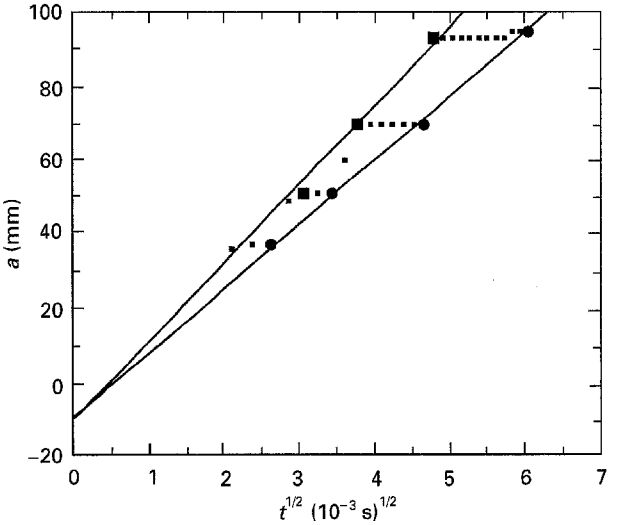

Figure 16 Crack length versus root time data for the PEEK/carbon-fibre composite at a test rate of 1.1 m s^{-1}. (●) Crack initiation, (■) crack arrest, (■) points at which crack remains stationary.

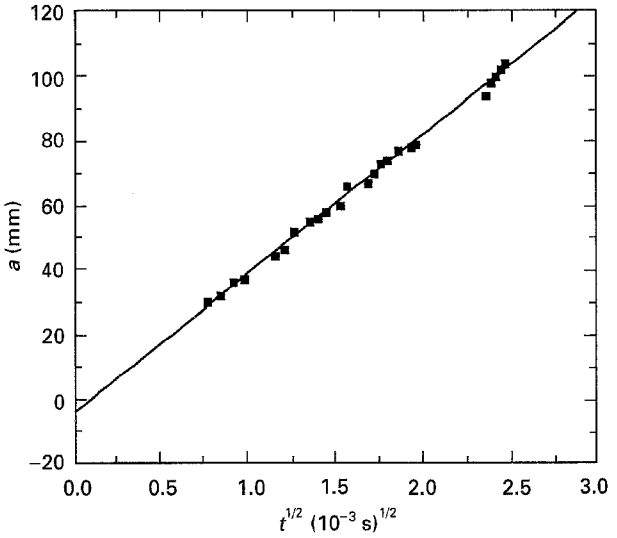

Figure 17 Crack length versus root time data for the PEEK/carbon-fibre composite at a test rate of 6.5 m s^{-1}. The linear fit to the data yields a correlation coefficient of 0.996.

was stable. In this section, the analysis will be applied to the experimental data recorded for the PEEK/carbon-fibre composite which showed stick–slip crack growth. Other materials which exhibit stick–slip crack growth, e.g. the bonded joints described in Part I [1] may be analysed in a similar manner, as will be shown in Section 5.

4.2. Interpretation of stick–slip experimental data via the dynamic analysis

It was shown in Part I [1] that the PEEK/carbon-fibre composite and the adhesive joints bonded with toughened epoxy adhesives exhibited stick–slip crack growth at all test speeds above a critical rate. However, as the test speed was increased past this rate, the steps in the crack-growth profile became smaller and more numerous until at the fastest test rates, it became practically impossible to identify on the high-speed films the points of crack initiation and arrest. Indeed, at rates faster than 10 m s^{-1}, the crack length versus time data for the PEEK/carbon-fibre composite appeared to be stable and continuous. The main difficulty in analysing these data therefore lies in correctly defining the values of G_1 and G_2 at each test rate.

Fig. 16 shows the a versus $t^{1/2}$ data for the PEEK/carbon-fibre composite at a test rate of 1.1 m s^{-1}. These data do not lie on a single line and hence a different approach to their analysis is required. By defining G_2 as the value of G at crack initiation as before, and now defining G_1 as the value G at crack arrest, the initiation and arrest points may be fitted separately to determine a value of A associated with initiation and a value of A associated with crack arrest. In this test, the initiation and arrest points are well defined. However, as the test rate is increased to 6.5 m s^{-1}, the majority of the a versus $t^{1/2}$ data lie on a straight line with a correlation coefficient of 0.996, as may be seen in Fig. 17. By removing the clearly defined points at crack arrest, these data may now be treated as propagation data

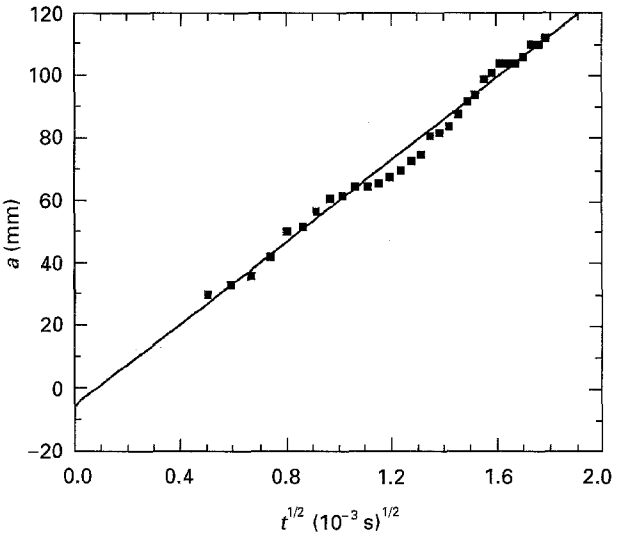

Figure 18 Crack length versus root time data for the PEEK/carbon-fibre composite at a test rate of 14.9 m s^{-1}. The linear fit to the data yields a correlation coefficient of 0.987.

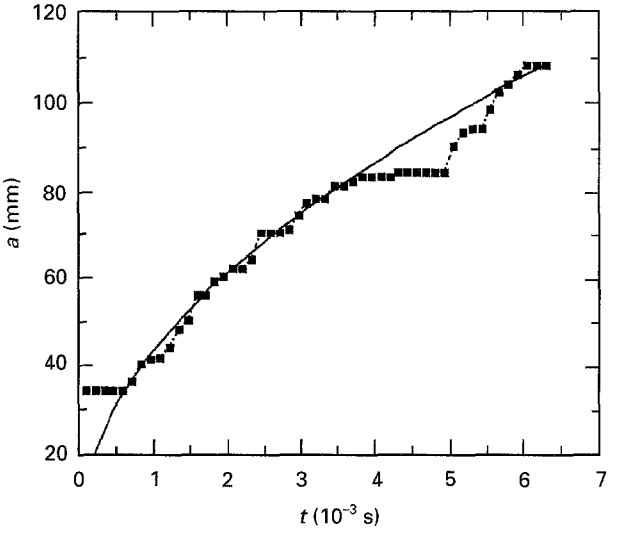

Figure 19 Crack length versus time data recorded for the the PEEK/carbon-fibre composite at a test rate of 6.5 m s^{-1}. Data points represent the corrected crack length values. (——) Values predicted by steady-state theory.

TABLE III Experimental values of A, Δ and t_0 for the PEEK/carbon-fibre composite at increasing test rates with the corresponding values of G_1 and G_2

Test rate (m s^{-1})	Expt. A (mm (ms)$^{-1/2}$)	Δ (mm)	Expt. t_0[a] (ms)	G_1 (J m^{-2}) (Eq. 20)	G_2 (J m^{-2}) (Eq. 40)
1.10	16.1	2.0	3.81 ± 0.62	458[b]	757[b]
6.50	43.2	4.4	0.66 ± 0.06	515	610
14.90	65.7	6.0	0.30 ± 0.05	476	550
18.40	72.7	8.5	0.30 ± 0.05	527	570

[a] Errors represent the high-speed camera framing interval.
[b] These values obtained by plotting repeated initiation and arrest values separately, then using Eq. 20.

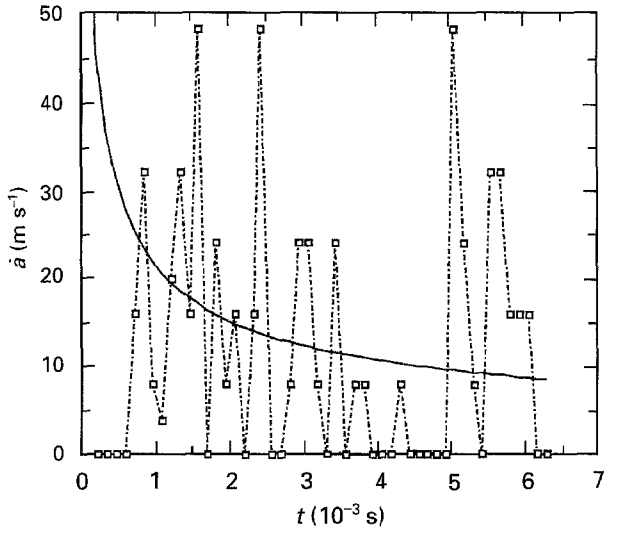

Figure 20 Crack velocity versus time data recorded for the the PEEK/carbon-fibre composite at a test rate of 6.5 m s^{-1}. Data points represent the experimental values. (——) Values predicted by steady-state theory.

and a linear fit to them enables G_1 to be calculated. Because it was not possible to define precisely the points of repeated crack initiation, G_2 was determined using the same technique as was used for the epoxy/carbon-fibre composite earlier i.e. by using the measured initiation time, t_0, and Equations 40 and 41. Fig. 18 shows the a versus $t^{1/2}$ data for the PEEK/carbon-fibre composite when tested at 14.9 m s^{-1}. The values of A, Δ, t_0, G_1 and the corresponding values of G_2 are shown in Table III for the PEEK/carbon-fibre composite at four different test rates between 1.1 and 18.4 m s^{-1}.

The trend for the value of G_2 to decrease while the value of G_1 increases with rate can be seen in Table III, and was also reported in Part I. As the values of G_1 and G_2 approach one another, the value of β approaches unity (see later, Table IV) and so the underlying cause of stick–slip crack propagation is removed.

4.3. Relationship between the experimental data and the steady state

As the test rate was increased above 1 m s^{-1}, the crack propagation in the PEEK/carbon-fibre composite became more continuous and therefore followed the steady state more closely. It will be shown in the next section that the approximate arrest points can be predicted during the test at 1 m s^{-1} provided the dynamic parameters β and ε are known. For test rates higher than 6 m s^{-1}, it was possible to compute the steady state values of a and $\dot{a}$ because a value of A relating to crack propagation could be defined, as shown in Table III. These values are shown in Fig. 19 and 20 for a test at 6.5 m s^{-1} and in Figs 21 and 22 for a test at 14.9 m s^{-1}. The corrected experimental values are shown as the points, and the steady-state values are shown as the solid lines. However, it was not possible to analyse the test at 1.1 m s^{-1} in this manner, because the A value defined for this test was not for propagation, but for arrest.

4.4. Use of the transient analysis to predict the crack-growth behaviour

The parameters t_0, β and ε required for the model are shown in Table IV for the PEEK/carbon-fibre

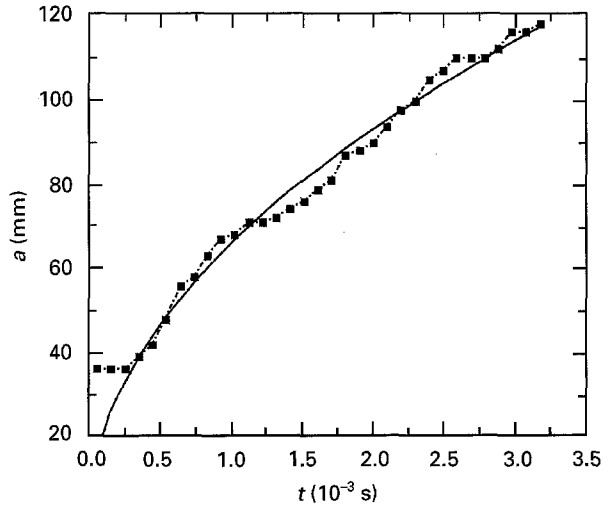

Figure 21 Crack length versus time data recorded for the PEEK/carbon-fibre composite at a test rate of 14.9 m s^{-1}. Data points represent the corrected crack length values. (——) Values predicted by steady-state theory.

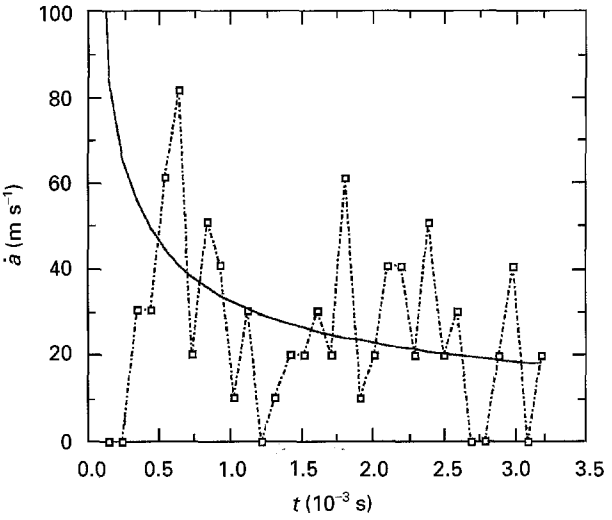

Figure 22 Crack velocity versus time data recorded for the PEEK/carbon-fibre composite at a test rate of 14.9 m s^{-1}. Data points represent the experimental values. (——) Values predicted by steady-state theory.

TABLE IV Calculated values of t_0, β and ε for the PEEK/carbon-fibre composite as the test rate is increased

Test rate (m s^{-1})	t_0	β (Eq. 41)	ε (Eq. 32)	ε (Best fit)
1.10	5.35	1.134	82.29	58.20
6.50	0.687	1.042	14.67	10.42
14.90	0.318	1.031	6.30	4.56
18.40	0.350	1.012	5.33	3.89

composite. As the test rate was increased above 1 m s^{-1}, it was noted that the value of G_2 decreased while the value of G_1 increased somewhat. This resulted in a decreasing β with increasing test rate which is consistent with the observation that the crack propagation becomes more continuous at higher rates. It was again necessary to account for the loss of

TABLE V Crack arrest conditions for the PEEK/carbon-fibre composite as a function of test speed

Test rate (m s^{-1})	$\frac{G_2}{G_1}$	$\left(1+\frac{1.2}{\varepsilon^2}\right)$	Stick–slip behaviour	
			Predicted	Seen in test?
1.10	1.65	1.00	Yes	Yes
6.50	1.18	1.01	Yes	Yes
14.90	1.16	1.06	Yes	No
18.40	1.08	1.08	No	No

symmetry in the DCB at high speeds by using a best fit value of ε as shown in Table IV.

Section 2 described how the arrest conditions could be predicted provided that G_1, G_2 and ε were known. An approximate guide to whether the crack will arrest during a test may be deduced via Equation 45; i.e. if the condition is satisfied, then crack arrest will occur during the test.

Table V explores this condition over a range of test speeds up to 18.40 m s^{-1} and shows the decreasing tendency for crack arrest to occur during a DCB test on the PEEK/carbon-fibre composite as the test rate is increased above 1 m s^{-1}. It also shows that this simple analysis predicts stick–slip type crack growth at rates of up to about 15 m s^{-1}, after which continuous crack growth is seen; i.e. stick–slip crack growth is observed if the condition in Equation 45 is satisfied.

Further, the dynamic theory enabled the repeated arrest crack lengths, $\bar{a}_{1,2\ldots n}$ to be predicted. For the test at 1.1 m s^{-1}, $a_0 = 34$ mm and a value of $\beta = 1.134$ may be taken from Table IV, a first crack arrest length may be predicted at 38.5 mm. Experimental test data show that the first arrest point occurred at a crack length of 37 mm. Hence the corrected value, i.e. $(a + \Delta)$ is 39 mm, as $\Delta = 2$ mm for this test. This value is in very close agreement to the predicted value. Clearly as β decreases, the amount of crack propagation prior to arrest decreases, resulting in the observed narrower stick–slip bands. However, when β falls below the critical level, stick–slip crack growth will not occur.

Figs 23 and 24 show values of p/a_0 and $\dot{p}t_0/a_0$ for the PEEK/carbon-fibre composite tested at 6.5 m s^{-1}. It was evident from Figs 19 and 20 that during this test there was a period of crack arrest lasting almost 1 ms. Although earlier points of crack arrest do occur, these last for very short durations and consequently the crack propagation during this period can be treated as continuous without introducing significant error. Hence, although the measured crack behaviour followed the steady state quite closely up to this point, beyond this point a large deviation occurred. It was therefore necessary to treat the test as two distinct periods of crack growth. Therefore, by computing Equations 38 and 39 from the instant of crack initiation to the first instant of crack arrest, then stopping and restarting the computation at the second instant of crack initiation until the end of the test, Figs 23 and 24 show that quite an accurate prediction of the crack length and crack velocity behaviour is obtained.

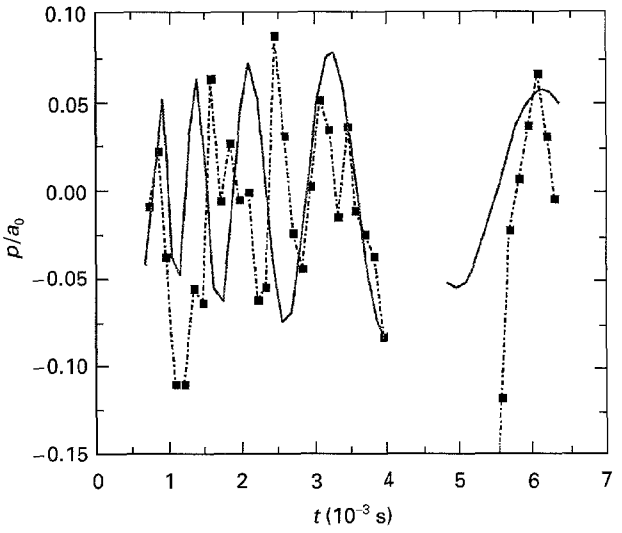

Figure 23 Values of p/a_0 versus time for the PEEK/carbon-fibre composite at a test rate of $6.5\,m\,s^{-1}$. The data points are the experimental values. (——) Equation 38.

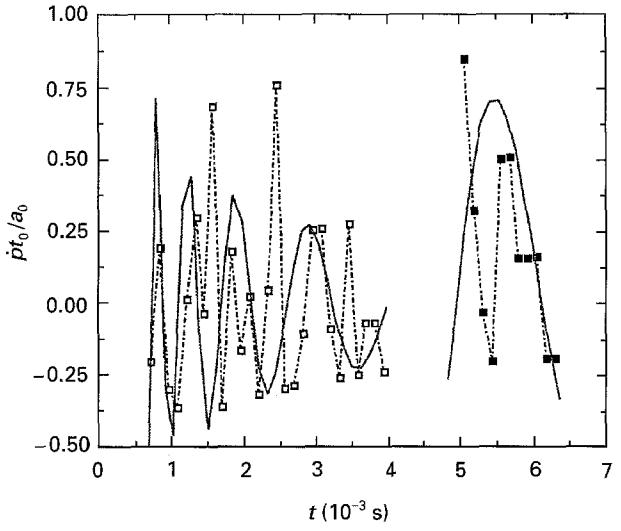

Figure 24 Values of $\dot{p}t_0/a_0$ versus time for the PEEK/carbon-fibre composite at a test rate of $6.5\,m\,s^{-1}$. The data points are the experimental values. (——) Equation 39.

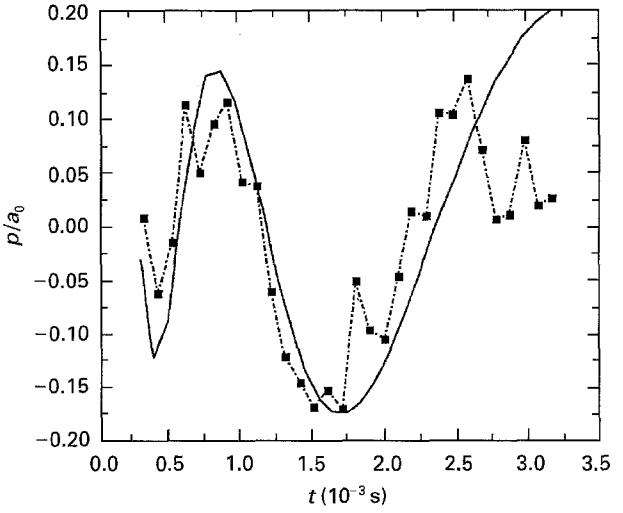

Figure 25 Values of p/a_0 versus time for the PEEK/carbon-fibre composite at a test rate of $14.9\,m\,s^{-1}$. The data points are the experimental values. (——) Equation 38.

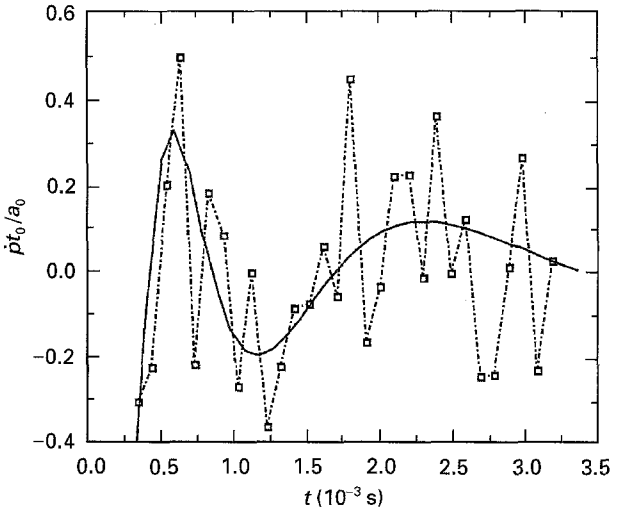

Figure 26 Values of $\dot{p}t_0/a_0$ versus time for the PEEK/carbon-fibre composite at a test rate of $14.9\,m\,s^{-1}$. The data points are the experimental values. (——) Equation 39.

Finally, Figs 25 and 26 show the values of p/a_0 and $\dot{p}t_0/a_0$ for the PEEK/carbon-fibre composite tested at a rate of $14.9\,m\,s^{-1}$. As no extended period of crack arrest occurred during this test, the data were treated as continuous. Indeed, it can be seen that the good agreement exists between the experimental values of p/a_0 and $\dot{p}t_0/a_0$ and the computed values.

5. Analysis of the experimental test data obtained when testing the adhesively bonded carbon-fibre composites (stick–slip crack growth)

5.1. Introduction

It was shown in Part I how the epoxy/unidirectional carbon-fibre composite beams were bonded with one of two rubber-toughened epoxy adhesives to form adhesively bonded DCBs. When tested at rates of up to about $15\,m\,s^{-1}$, it was shown that the value of G_{Ic} remained approximately constant when an epoxy-film adhesive was employed (FM73M from American Cyanamid) but when an epoxy-paste adhesive was employed (EA9309 from Hysol Dexter) the value of G_{Ic} decreased by 40% at $10\,m\,s^{-1}$ relative to the static value. The measured crack length versus time data recorded for a number of these tests will now be analysed using the dynamic analysis.

5.2. Interpretation of the experimental data

To investigate the dynamic behaviour of the adhesively bonded joints, test data recorded at rates of about 1 and $10\,m\,s^{-1}$ have been analysed for each adhesive. It was noted in Part I that joints bonded with either adhesive failed in a continuous manner at slow test rates, but as the test rate was increased above a critical rate, the continuous crack growth gave way to stick–slip crack growth.

A typical set of a versus $t^{1/2}$ data recorded at $1.4\,m\,s^{-1}$ is shown in Fig. 27 for a joint bonded with

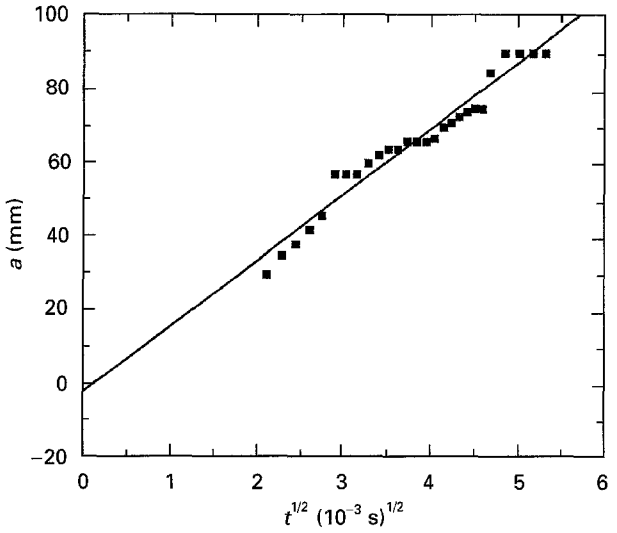

Figure 27 Crack length versus root time data for a joint bonded with the epoxy-film adhesive and tested at a rate of 1.4 m s^{-1}. The linear fit to the data yields a correlation coefficient of 0.956.

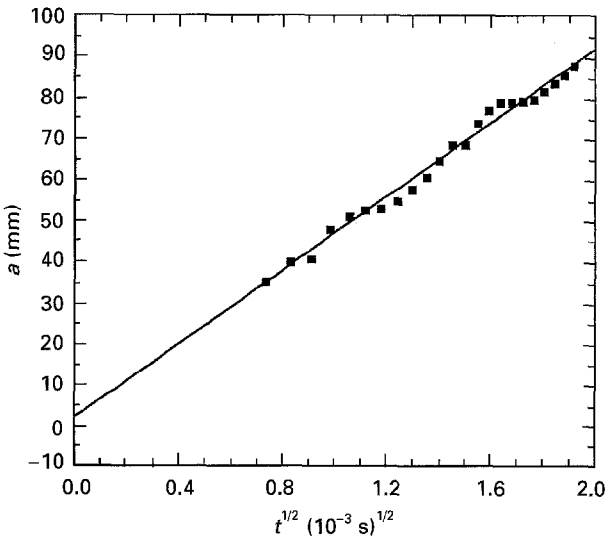

Figure 28 Crack length versus root time data for a joint bonded with the epoxy-film adhesive and tested at a rate of 10.1 m s^{-1}. The linear fit to the data yields a correlation coefficient of 0.988.

the epoxy-film adhesive. It can be seen that this data lies approximately along a straight line, with a correlation coefficient of 0.956, and hence the gradient, A, may be determined as well as the negative intercept, Δ. For this test at 1.4 m s^{-1}, $A = 18$ mm (ms)$^{-1/2}$ and $\Delta = 2.8$ mm. These values are shown in Table VI, together with the measured crack initiation time, t_0, and calculated values of G_1 and G_2 deduced via Equations 20 and 40, respectively. Fig. 28 shows the equivalent data recorded at a test rate of 10 m s^{-1}. The linear fit to these data is better, with a correlation coefficient of 0.988. The values of A, Δ and t_0 are again shown in Table VI, along with the calculated values of G_1 and G_2.

Fig. 29 shows a typical set of a versus $t^{1/2}$ data recorded at a test rate of about 1 m s^{-1} for a joint bonded with the epoxy-paste adhesive. These data are not linear, owing to the extended periods of crack arrest that were recorded during this test and therefore the data may not be fitted to a single line. However, it was shown in Section 4 that stick–slip crack growth can be analysed by considering the initiation and arrest points separately. The two lines drawn on Fig. 29 represent the best fit lines to the initiation and arrest data. The gradient of the line through the initiation points yields a value for G_2 and the gradient of the line through the arrest points yields a value for G_1. The data points recorded when the crack remained stationary were disregarded. This procedure was repeated for the data obtained at a test rate of

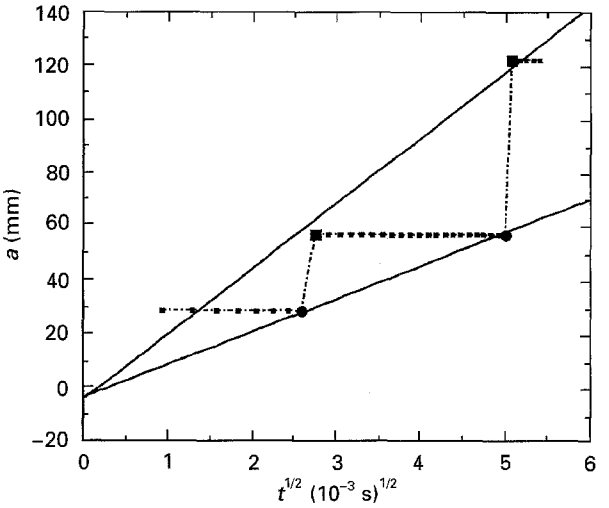

Figure 29 Crack length versus root time data for a joint bonded with the epoxy-paste adhesive and tested at a rate of 1.1 m s^{-1}. (●) Initiation, (■) arrest, (■) points at which the crack remains stationary.

14.7 m s^{-1} and the resulting values of A, Δ, G_1 and G_2 are shown in Table VI.

From Table VI it can be seen that the value of G_{Ic} at crack initiation, $\equiv 2G_2$, measured for the joints bonded with the epoxy-film adhesive decreases by about 10% as the test rate is increased from 1 m s^{-1} to 10 m s^{-1}. However, the joints bonded with the epoxy-paste adhesive show a much more significant

TABLE VI Experimental values of A, Δ and t_0 for the adhesive joints at different test rates with the corresponding values of G_1 and G_2

	Test rate (m s^{-1})	Expt. A (mm (ms)$^{-1/2}$)	Δ (mm)	Expt. t_0^a (ms)	G_1 (J m^{-2})	G_2 (J m^{-2})
Film	1.4	18.0	2.8	4.83 ± 0.40	957	1294
Film	10.1	45.2	−1.7	0.57 ± 0.07	1012	1168
Paste	1.1	24.4	4.8	7.08 ± 0.42	105	1665
Paste	14.7	72.1	1.0	0.25 ± 0.20	359	954

[a] Errors represent the high-speed camera framing interval.

reduction in the value of G_2 which decreases by about 42% over a similar range of test rates. It is of interest to note that the value of G_1 remains approximately constant for the joints bonded with the epoxy-film adhesive over this range, but the joints bonded with the epoxy-paste adhesive show a three-fold increase in this value.

5.3. Relationship between the experimental data and the steady state

The steady-state values of the crack length and crack velocity may be obtained for the adhesive joints using the procedure described previously in Section 3.3. When the a versus $t^{1/2}$ data are linear, the gradient A may be used to deduce these steady-state values. Figs 30 and 31 show the experimental and steady-state values of a and $\dot{a}$ for a joint bonded with the epoxy-film adhesive and tested at the rate of 1.4 m s^{-1}. When the a versus $t^{1/2}$ data are not linear due to extended periods of crack arrest as was observed when testing joints bonded with the epoxy-paste adhesive, the steady state is not followed and it becomes necessary to consider each period of crack growth separately, as was discussed in Section 4.4.

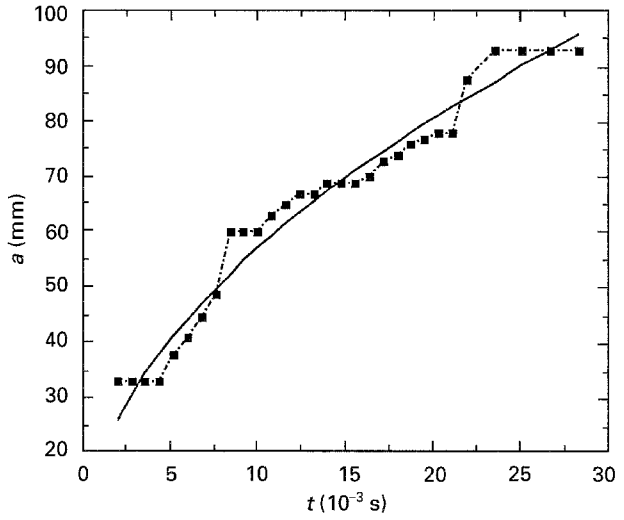

Figure 30 Crack length versus time data for a joint bonded with the epoxy-film adhesive and tested at a rate of 1.4 m s^{-1}. Data points represent the corrected crack length values. (——) Values predicted by steady-state theory.

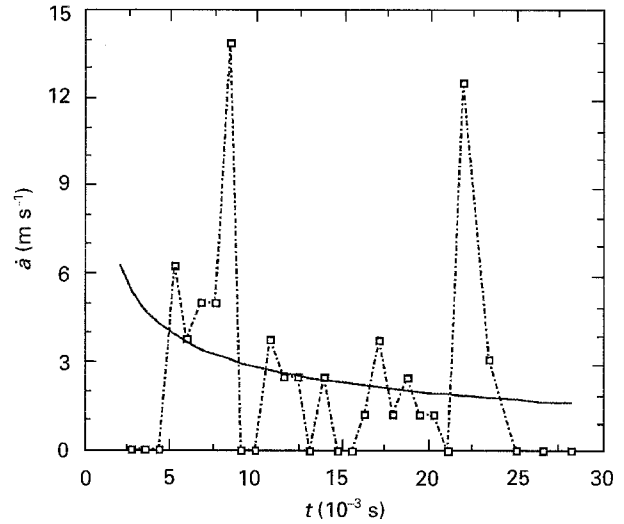

Figure 31 Crack velocity versus time data for a joint bonded with the epoxy-film adhesive and tested at a rate of 1.4 m s^{-1}. Data points represent the experimental values. (——) Values predicted by steady-state theory.

TABLE VII Calculated values of t_0, β and ε for the adhesively bonded joints

Adhesive	Test rate (m s^{-1})	t_0	β (Eq. 41)	ε (Eq. 32)	ε (Best fit)
Film	1.4	4.350	1.078	90.83	45.0
Film	10.1	0.571	1.035	13.20	7.5
Paste	1.1	7.580	1.995	43.25	N/A
Paste	14.7	0.276	1.260	05.43	N/A

5.4. Use of the transient analysis to predict the crack-growth behaviour

The parameters t_0, β and ε required for the analysis are shown in Table VII for the adhesive joints. The table shows values for joints bonded with both the epoxy-film and the epoxy-paste adhesives. It is of interest to note that significantly higher values of β were recorded for the joints bonded with the epoxy-paste adhesive than for those bonded with the epoxy-film adhesive. The degree of stick–slip crack growth is clearly greater when β is large (see Equation 45), and it was noted that as the test rate was increased the general trend was for G_2 to decrease and for G_1 to increase. Thus a large G_2 relative to G_1 favours stick–slip crack growth and as the rate was increased above 1 m s^{-1} the value of β decreased for both adhesives and hence it can be seen that the crack growth becomes more continuous at the highest rates. It was again necessary to adjust the value of ε to account for the loss of symmetry in the high-rate DCB test. The values of ε calculated by Equation 32 and those values which gave the best fit between the experimental data and Equations (38) and (39) are also shown in Table VII.

Figs 32 and 33 show the computed and experimental values of p/a_0 and $\dot{p}t_0/a_0$ as a function of time for a joint bonded with the epoxy-film adhesive and tested at 10.1 m s^{-1}. It can be seen that Equations 38 and 39 quite accurately predict the measured crack-growth behaviour for this test. The high values of β calculated for joints bonded with the epoxy-paste adhesive predict stick–slip crack growth will occur and hence all the growth will take place in short bursts.

6. Conclusion

It has been shown how dynamic expressions for the mode I fracture toughness, G_{Ic}, may be derived for a high-rate DCB test. It was shown that there are two expressions for the kinetic energy, one prior to crack initiation when $\dot{a} = 0$ and one after initiation when $\dot{a} > 0$. It was therefore shown that the G required for

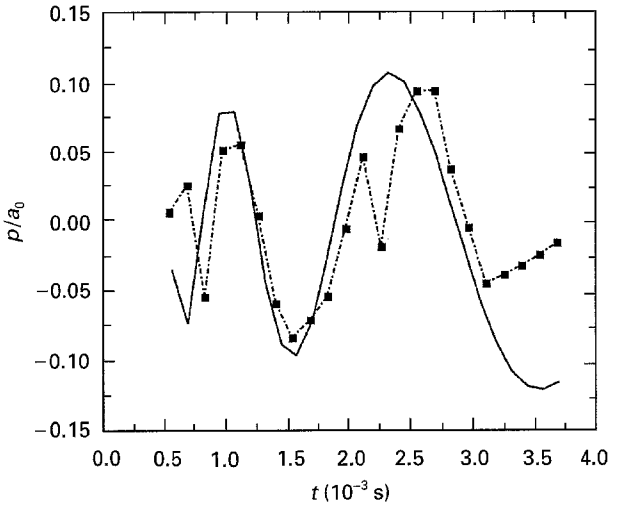

Figure 32 Values of p/a_0 versus time for a joint bonded with the epoxy-film adhesive and tested at a rate of 10.1 m s^{-1}. Data points are the experimental values. (——) Equation 38.

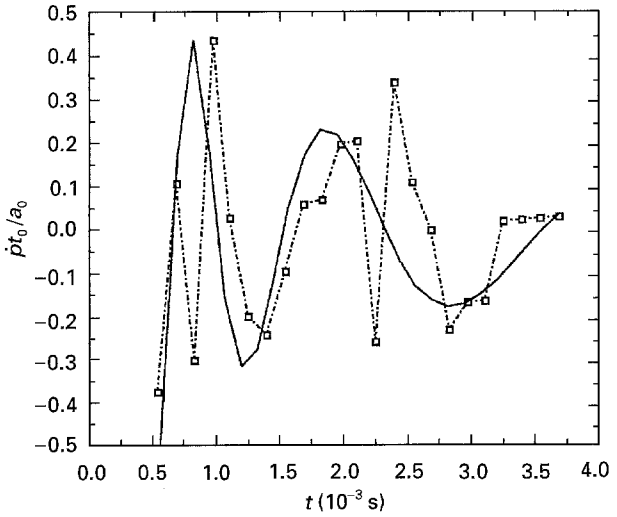

Figure 33 Values of $\dot{p}t_0/a_0$ versus time for a joint bonded with the epoxy-film adhesive and tested at a rate of 10.1 m s^{-1}. Data points are the experimental values. (——) Equation 39.

steady-state propagation was less than the G required for crack initiation. Hence it was shown that after initiation, there would be a transition growth region and mismatch in the boundary conditions before the crack reached the steady state. This transitory region constitutes the major dynamic effect in the DCB test and details of this were investigated by considering small perturbations from the steady state. The perturbations observed in the measured crack length and crack velocity values were large at high test rates and it was demonstrated for two carbon-fibre composites and two adhesively bonded carbon-fibre composites how these variations could be predicted.

The values of the perturbations were deduced from the experimental data and it was shown that, although the magnitude of the kinetic energy component was usually small compared to the fracture toughness, G_{Ic}, the dynamic crack-length variations from the steady state caused oscillations in the measured values of G_{Ic}. Values of G_{Ic} deduced under assumed steady-state conditions gave close agreement with values reported in Part I [1] of this series of papers. Higher values of G_{Ic} at crack initiation were noted, however, for the epoxy/carbon-fibre composite and, although this was considered to be an artefact of the high rate test, it was found necessary to include this in the model. The analysis has also predicted quite accurately the transient crack-growth behaviour which was measured during the high-rate tests, although an adjustment to the model was necessary to account for the loss of symmetry experienced at the higher test rates.

In Part III [8], the experimental results from the mixed-mode and mode II loading at high test rates will be discussed in detail.

Acknowledgements

The authors thank the Engineering Physical Sciences Research Council for financial support and the Polymer Engineering Group, ICI plc, and Ciba Composites, for general support.

References

1. B. R. K. BLACKMAN, J. P. DEAR, A. J. KINLOCH, H. MacGILLIVRAY, Y. WANG, J. G. WILLIAMS and P. YAYLA, *J. Mater. Sci.* **30** (1995) 5885.
2. Y. WANG and J. G. WILLIAMS, *Composites* **25**(5) (1994) 323.
3. J. G. WILLIAMS, *Eur. J. Mech. A/Solids* **13**(4-suppl.) (1994) 227.
4. S. HASHEMI, A. J. KINLOCH and J. G. WILLIAMS, *Proc. R. Soc. Lond. A* **427** (1990) 173.
5. J. G. WILLIAMS, *Strain Anal. Eng. Design* **28**(4) (1993) 237.
6. J. P. BERRY, *J. Mech. Phys. Solids* **8**(3) (1960) 194.
7. *Idem, Ibid.* **8** (3) (1960) 207.
8. B. R. K. BLACKMAN, A. J. KINLOCH, H. MacGILLIVRAY, Y. WANG, J. G. WILLIAMS and P. YAYLA, *J. Mater. Sci.* **31** (1996) 4467.

Received 19 January
and accepted 18 March 1996